

NMR investigation of the electronic structure of expanded liquid cesium

W. W. Warren, Jr. and G. F. Brennert
AT&T Bell Laboratories, Murray Hill, New Jersey 07974

U. El-Hanany
Soreq Nuclear Research Center, Yavne, Israel
(Received 6 September 1988)

We describe a comprehensive study of the ^{133}Cs Knight shift and nuclear relaxation rates in liquid cesium from the vicinity of the melting point to the critical region of the liquid-gas transition. The data cover a temperature range 55–1590°C at pressures up to 90 bars and include a wide range of sample densities from 0.70 to 1.93 g/cm³. Measurements extended to pressures of 900 bars in the lower part of the temperature range. The data yield the isobaric temperature dependence, the isothermal pressure dependence, and the isochoric temperature dependence of the Knight shift as well as the isobaric temperature dependence of the nuclear relaxation rate. At low densities, a strong enhancement of the Knight shift was observed which is related to enhancement of the static susceptibility. In the range of increasing enhancement of the shift and susceptibility we observed strong deviations of the relaxation rate from the Korringa relation signifying breakdown of the conventional Stoner model of exchange-correlation enhancement. The charge density at the nucleus exhibits a surprising decrease with decreasing density in the range 0.8–1.4 g/cm³. These effects lead to a description of expanded cesium as a highly correlated metal with incipient antiferromagnetic spin correlations between electrons on neighboring ions.

I. INTRODUCTION

The electronic structure and properties of a monovalent element subject to large changes in density occupy a central place in condensed matter physics. Despite their apparent simplicity, these “half-filled band” metals are strongly influenced by the effects of electron-electron interactions. In a seminal paper, Mott¹ showed that one-electron band theory eventually breaks down on expansion of a monovalent crystalline metal due to the loss of long-range screening of the ionic potentials. The result is an insulating state with one electron localized on each atomic site. Subsequent work by Hubbard² based on a model introduced by Anderson³ showed that short-range interactions represented by the intra-atomic Coulomb repulsion U also lead to an insulating state for U sufficiently large compared with the bandwidth W . Similar considerations come into play when one considers the compression of hydrogen which is predicted to become metallic at sufficiently high pressures⁴ although this case is complicated by the transition of hydrogen from the molecular to the atomic form. Providing still another example of its generality, the half-filled band Hubbard model forms the starting point for many current theories of high-temperature superconductivity.⁵

The magnetic properties of monovalent metals are particularly sensitive to the effects of electron-electron interactions. Even at ordinary densities, the uniform, static susceptibilities of the alkali metals are enhanced significantly by exchange-correlation effects. The enhancements lie in the range 1.5–2.0 and are usually described in terms of the Stoner model.⁶ Close to the metal-nonmetal transition where the ratio U/W becomes large, Brinkman and

Rice,⁷ using a method designed by Gutzwiller,⁸ showed that correlation leads to further enhancement. Their result is expressed as an enhancement of the effective mass and, unlike the Stoner effect, both the paramagnetic susceptibility and electronic specific heat are enhanced. The ground state of such a “highly correlated metal” is predicted to be antiferromagnetic on the Hubbard model.⁹ Similarly, several calculations using density-functional theory have shown that the ground state of metallic, atomic hydrogen should be antiferromagnetic.^{10–12} The energies of the ferromagnetic and antiferromagnetic states are much closer for the alkali metals, and calculations differ as to which would form first in an expanded crystalline alkali metal.^{11,13}

Despite the importance for theory of the concept of an expanded monovalent crystal, such a system cannot be realized experimentally in a single-component solid. However, large reductions of density can be obtained for liquid alkali metals using thermal expansion as the metal is heated to the region of the liquid-gas critical point. The range of possible density variation can be seen, for example, from the temperature-density phase diagram^{14–16} of cesium shown in Fig. 1. Reduction of the density by about a factor of 5 is possible in the subcritical liquid and arbitrarily low densities are possible in the supercritical fluid. Studies of the electrical conductivity of the alkali metals have established that a continuous metal-nonmetal transition occurs on passing through the critical region.^{17–20} Because of this transition, the interparticle forces are strongly affected by changes in density. This has important consequences for the liquid-gas equilibrium. Early speculations by Landau and Zeldovich²¹ on the interplay between the metal-nonmetal and liquid-

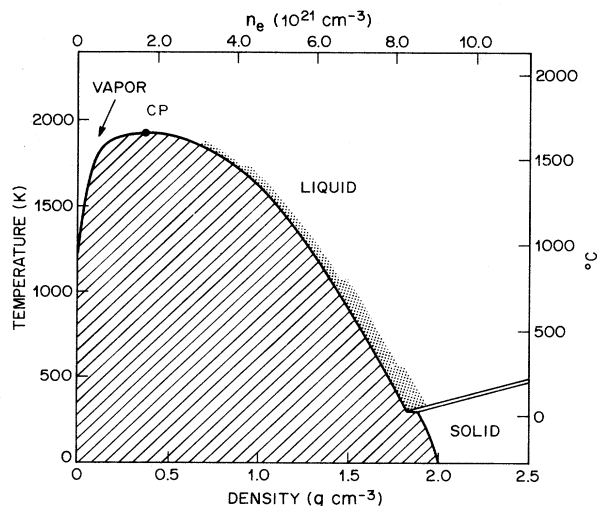


FIG. 1. Temperature-density phase diagram of cesium (Ref. 14–16). Fine shading indicates regions studied in this investigation. Upper scale shows the electron density for one electron/atom.

gas transitions, have taken explicit form in recent studies of singularities in the rectilinear diameters of metals.^{16,22}

Measurements of the static magnetic susceptibility of Cs and Rb show strikingly increased enhancement in the low-density metal.^{23,24} Interpretation of this effect in terms of models of expanded monovalent crystals is complicated by liquid-state disorder and the high temperatures at which the experiments are carried out. A particular consequence of the latter is limitation of the susceptibility below the Curie value at high temperatures.²⁵ This is a clear demonstration that the low-density enhancement is a mass enhancement of the type considered by Brinkman and Rice, rather than enhancement of the Stoner type.²⁵

The inability to approach the $T=0$ limit is an obvious disadvantage of the study of expanded alkali metals. There are, however, compensating advantages. Chief among these is the absence of matrix and solvation effects which are inevitably present in low-density metals produced by solution of a metal in a nonmetal, i.e., Si:P, metal-NH₃, Cs-Xe films, etc. All such systems are disordered, but liquid systems enjoy the advantage of thermodynamic equilibrium and motional averaging of local inhomogeneities on the time scale of most experimental probes. This is particularly important for highly local probes such as nuclear magnetic resonance.

In this paper we describe a comprehensive investigation of expanded liquid cesium using nuclear magnetic resonance (NMR). Our measurements extend from the vicinity of the normal melting point (T_m) to the critical region of the liquid-gas transition ($T_c = 1651^\circ\text{C}$, $P_c = 92.5$ bars). The density varies by a factor of roughly 2.7 over our experimental range and at the highest temperature reached, $(T_c - T)/T_c = 3 \times 10^{-2}$. We have measured Knight shifts, obtaining information about the behavior of the uniform, static susceptibility and the electronic

charge density at the nucleus, and the linewidth (free-induction decay lifetime), related to the low-frequency limit of the integrated nonuniform susceptibility. Some of these data have been reported previously in preliminary and partial form.^{26–28} Our experimental apparatus, discussed in the next section, permits measurement of the pressure dependence of these quantities at constant temperature at all but the highest temperatures attained. Although the measurements approached the critical temperature, all data reported in this paper were obtained within the metallic range of expanded cesium. The data reveal remarkable changes in electronic character due to electron-electron interactions in the low-density metal. These are reflected in the real and imaginary parts of the generalized magnetic susceptibility and in the distribution of conduction electron charge.

II. EXPERIMENTAL TECHNIQUES

A. High-temperature–high-pressure NMR apparatus

The fundamental experimental requirement for this investigation was a means of maintaining a sample of liquid cesium at temperatures and pressures up to the critical conditions in a uniform static magnetic field and in a suitable radio-frequency coil for NMR measurements. The system shown schematically in Fig. 2 provides the necessary environment for NMR studies and offers an additional capability for simultaneous measurement of the sample density. The basic element is an internally heated Be-Cu autoclave in which the cesium sample is maintained in a single-crystal sapphire cell within the high-temperature zone. The pressure medium in the autoclave is high-purity argon gas. Pressure balance between the cell interior and the autoclave pressure was achieved externally by pressurizing the column of liquid cesium leading to the cell. Liquid cesium was separated from the argon by a length of capillary tube containing decane and by liquid mercury in a U tube. The height of the mercury in the U tube, detected by a magnetic float and external

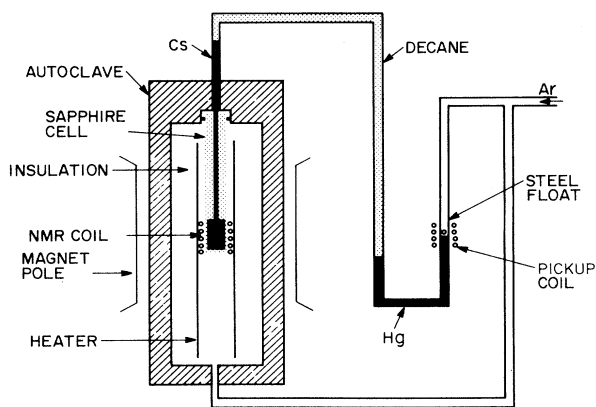


FIG. 2. Schematic diagram of apparatus for high-temperature–high-pressure NMR measurements on liquid cesium.

inductive pickup, provided a measure of the cesium density. Circulating water cooling the exterior surface of the autoclave was maintained at 55 °C in order that the cesium remain in the liquid state at pressures up to 900 bars.

An alumina ceramic tube (length 120 mm, outside diameter 18 mm) supported three independent heating elements wound noninductively in "zigzag" form. The wire utilized for these elements was either molybdenum (0.5 mm) or, for the highest temperatures, tungsten (0.8 mm). Current for the heating elements was provided by three separate regulated dc power supplies. The insulation separating the elements from the inner wall of the pressure vessel had to meet the conflicting requirements of low-thermal conductivity and low permeability to connecting currents of the dense argon pressure medium. For this purpose, we used a layered structure formed by rolled 0.025-mm molybdenum foil. The layers were separated with small spacing by 0.05-mm "pimples" embossed on the foil. With this insulation, the power requirement for a sample temperature of 1500 °C at 90 bars was 450 W.

The working thermometers for these experiments comprised three tungsten-tungsten-rhenium thermocouples placed in the heater tube wall. Temperatures measured at three points along the heater tube were equalized by the power supplies to provide uniform temperature along the length of the tube and thus minimize the thermal gradient over the sample volume. We used the liquid-vapor transition of the cesium sample to calibrate the thermocouple closest to the sample. Three points were used to establish a smooth calibration curve: 26 bars, 1210 °C; 48 bars, 1393 °C; and 67 bars, 1520 °C. As an independent check of the temperature calibration, we measured the absolute density at 1590 °C and 90 bars and obtained agreement within 10 °C with the equation-of-state data of Hensel *et al.*²⁹ Pressures were measured with an accuracy of ± 1 bar.

B. Sample cell and NMR probe

The cell containing the cesium³⁰ sample consisted of a closed-end single-crystal sapphire tube³¹ of 9.5-mm outside diameter, 0.8-mm wall, and 127-mm length. The open end of the tube was sealed to the stainless-steel plug at the end of the autoclave by means of an "O ring." The cesium column continued outside the autoclave in high-pressure stainless-steel capillary tube (Fig. 2). A solid sapphire rod insert with a shallow longitudinal groove along one side occupied most of the internal volume of the sample tube thereby reducing the amount of cesium required. Only in the NMR sample space (0.85 cm³) at the closed end of the tube did cesium fill the tube to its full diameter. The insert rod fit snugly into the sample tube and the groove permitted liquid cesium to flow in and out of the sample volume during filling and subsequent density changes. With this arrangement, the cesium formed a "bulk" NMR sample and only nuclei within the skin depth of the cylindrical sample volume contributed to the signal. At the working frequency, the skin depth ranged from 0.12 mm at 55 °C to 0.7 mm at 1600 °C.

Sapphire was chosen for its high resistance to corrosion by liquid cesium. Nevertheless, after experiments above 1400 °C a light etching of the internal surface of the tube was apparent. While this indicated the dissolution of small amounts of oxide in the liquid cesium sample, we believe that constant exchange with the internal portions of the bulk sample minimized contamination of the active skin-depth region. Regular checks of the reproducibility of the ¹³³Cs Knight shift, a property very sensitive to dissolved oxide,³² confirmed that this was so.

The NMR coil was wound with 0.5-mm molybdenum or tungsten wire on an alumina form. The coil fit closely around the outside of the sapphire sample tube. Electrical leads to the coil were introduced into the high-pressure environment by means of feed throughs insulated with Vespel.³³ Butyl rubber gaskets provided the high-pressure seal around these leads. We experienced no problems with high-voltage radio-frequency breakdown as long as the gaskets were kept clean and dry.

C. Cell filling and cesium handling procedures

Considerable care was required to fill the sample tube safely with liquid cesium while avoiding contamination by exposure to oxygen. Cesium was transferred from an external stainless-steel reservoir. After connecting the reservoir to the apparatus, we evacuated the sample volume and connecting spaces, then injected liquid cesium from the reservoir under a pressure of about 1 bar. All parts of the experimental apparatus and reservoir were heated to keep the cesium molten throughout this operation. After transfer, we solidified the cesium and covered the top surface with decane for protection. Later, during final assembly, additional decane was added to separate the liquid cesium column from the liquid mercury in the U tube (Fig. 2).

Removal of cesium following an experimental run was carried out in a specially constructed glove box containing argon gas. By cooling the argon entering the glove box, we solidified all cesium in the system. The parts of the apparatus containing cesium could then be disassembled and placed into hexane without danger of spilling liquid metal. As a final step, cesium in the disassembled parts was oxidized in a controlled fashion by slowly adding ethanol to the hexane.

D. Density measurements

The mercury U tube shown in Fig. 2 provided a means of monitoring density changes while simultaneously conducting NMR measurements. The height of the mercury column directly reflected changes in the cesium density. The position of a small steel float on the mercury surface was detected inductively with a lock-in amplifier and a pickup coil on the outside of the high-pressure capillary. The lock-in output, in turn, controlled a stepping motor positioning the pickup coil to follow movement of the float and provide a digital readout of the column height. For calibration, we used the following expression to relate the density ρ to the column height h :

$$\rho = (A - h)/B \quad (1)$$

The constants A and B depend on pressure due to compression of decane in the column. At a given pressure, we determined A and B by comparison with the data of Franz¹⁵ at two temperatures (55 and 1000 °C). As a measure of the accuracy of the density measured at the highest temperatures, we compare our results with the measurements of Hensel *et al.*²⁹ who used the same vapor pressure scale for temperature calibration. At 1590 °C and 90 bars we obtained $\rho = 0.703 \pm 0.010$ g/cm³ compared with a value 0.720 ± 0.010 g/cm³ measured by those authors. Viewed as a discrepancy in temperature rather than density, this difference corresponds to 10 °C.

E. NMR techniques

NMR measurements were carried out with coherent, pulsed NMR techniques at a fixed frequency of 9.7 MHz. Typical pulse power produced a rotating radio-frequency (rf) magnetic field $H_1 = 90$ G and provided 90° rotation of the nuclear magnetization in 5 μ sec. Free-induction decays following single pulses were observed at repetition rates ranging up to 1 kHz. We took care to assure that heating of the sample by the rf pulses was negligible. A boxcar integrator recorded the integral of most of the free-induction decay as the magnetic field was swept through resonance. This method produces at the boxcar output a distorted mixture of absorption and dispersion in which the mixture depends on the phase of a reference signal and the distortion is due to the finite Fourier transform.³⁴ The distortion, in the form of oscillations in the wings of the resonance, grows increasingly severe as the free-induction decay lifetime shortens and becomes comparable with the dead time of the pulsed NMR spectrometer. Normally, the phase was set as close as practical to that giving a symmetric absorption signal. Data from repeated field sweeps were collected in a signal averager to improve the final signal-to-noise ratio.

Three examples of the averaged boxcar output are shown in Fig. 3. Comparison of these spectra reveals the two dominant general features of our results: (i) non-monotonic temperature dependence of the resonance position (shift) and (ii) strong broadening of the resonance as the temperature is increased. We utilized a computer program³⁵ with a nonlinear least-squares fit to extract the resonance position and free-induction-decay lifetime from data such as these. The fitting procedure automatically corrected for the finite transform distortion and phase error which are particularly apparent in Fig. 3(c).

Resonance shifts at various temperatures and pressures were measured relative to the resonance position at an easily reproduced reference point, 55 °C and 30 bars. In an independent measurement, we determined the value of the shift at this reference point to be $K = 1.472\%$ with respect to the ¹³³Cs resonance in dilute CsCl aqueous solution. This agrees well with previous measurements of the shift in liquid cesium near the melting point.³⁶⁻³⁸ The overall accuracy of the shift measurements depended strongly on temperature because of the temperature-dependent linewidth evident in Fig. 3. Shift accuracy ranged from $\pm 0.001\%$ at the lowest temperatures to $+0.02\%$ at the highest temperatures reached.

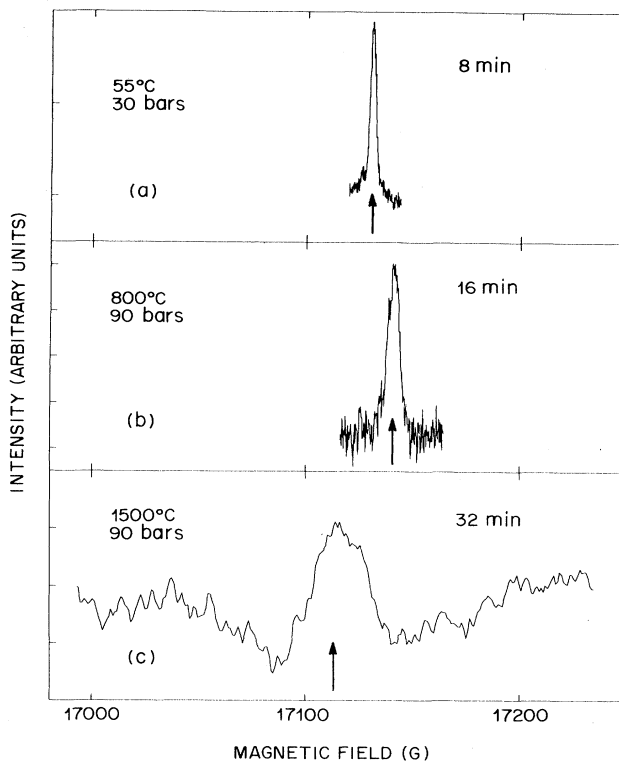


FIG. 3. ¹³³Cs NMR signals from liquid cesium at indicated temperatures and pressures. Signal acquisition times are indicated and arrows mark resonance positions determined by computer fit, including phase error correction.

We assume that the free-induction-decay lifetime $1/T_2^*$ extracted from the line-shape fit consists of two contributions: a term $1/T_1$ due to spin-lattice relaxation, dominant at most temperatures, and a contribution $(1/T_2)_in$ from the inhomogeneity of the magnetic field

$$1/T_2^* = 1/T_1 + (1/T_2)_in. \quad (2)$$

The contribution of inhomogeneous broadening was determined for each run by measurements at the reference point. Our independently determined value of $1/T_1$ at 55 °C and 30 bars corresponds to $1/T_1 T = 8.6 \pm 0.9$ (s K)⁻¹ in good agreement with the result $1/T_1 T = 8.4 \pm 0.4$ (s K)⁻¹ given by Kaeck³⁹ for liquid cesium at room temperature. We assume that the inhomogeneous contribution is independent of temperature, although its importance rapidly become negligible due to the rapid increase of $1/T_1$ with increasing temperature. At the very highest temperatures, an additional source of inhomogeneous broadening was introduced by the combined effects of the temperature gradient over the sample and the strong temperature dependence of the Knight shift. We determined the temperature gradient to be < 5 °C by observing the width of the vaporization and condensation transitions of our sample *in situ*. This translates into a linewidth contribution that is less than 10% of the observed value of $1/T_2^*$ in the high-

temperature range. Thus, the error introduced by temperature gradients is less than or, at worst, is comparable with the measurement precision under these conditions.

III. EXPERIMENTAL RESULTS

A. Knight shift

^{133}Cs Knight shifts were measured as a function of temperature under isobaric conditions. In Fig. 4 we present data for two pressures (90 and 120 bars) covering the full temperature range of this investigation. These results show an initial decrease in shift up to 600 °C followed by a strong increase as the temperature is raised to the critical region. Our complete data for all isobars are collected in Table I. The tabulated values represent averages over several runs and were derived from smoothed curves drawn through all the data obtained for each pressure.

The pressure dependence of the shift is shown explicitly in Fig. 5. We obtained these results by isothermal compression of the liquid at various temperatures. At 55° C we measured a logarithmic pressure coefficient

$$(\partial \ln K / \partial P)_{55} = 3.2 \pm 0.2 \times 10^{-5} \text{ bars}^{-1},$$

which agrees within experimental error with the value measured for the solid at 20 °C by Benedek and Kushi-da⁴⁰ (Table II). With increasing temperature, however, the pressure coefficient gradually decreases and changes sign in roughly the same temperature range as the minimum in the temperature dependence shown in Fig. 4. At higher temperatures, the pressure dependence becomes increasingly negative and we obtain, for example,

$$(\partial \ln K / \partial P)_{1190} = -15.9 \pm 3.5 \times 10^{-5} \text{ bars}^{-1},$$

for the shift coefficient at 1190 °C.

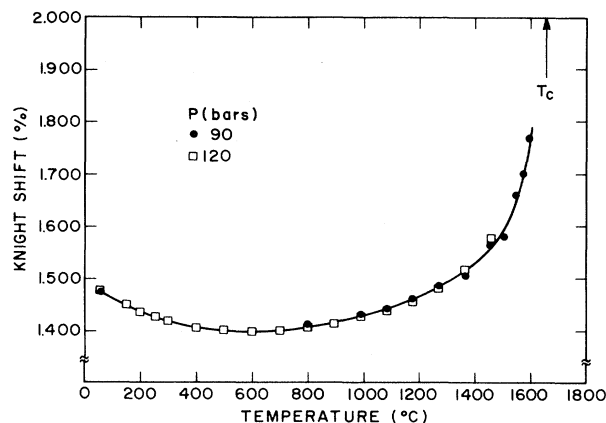


FIG. 4. Isobaric ^{133}Cs Knight shifts vs temperature for pressures of 90 and 120 bars.

The isobaric Knight-shift data are plotted against the density for various pressures in Fig. 6. This plot shows the variation of the shift over nearly a factor of 3 density change. The minimum density, 0.7 g/cm^3 , is slightly less than twice the critical density ($\rho_c = 0.379 \text{ g/cm}^3$). The minimum in the density dependence of the shift near 1.5 g/cm^3 corresponds to the minimum in the temperature dependence around 600 °C.

The relationship between the temperature and density dependences of the shift may be seen more clearly in Fig. 7 where the scales have been expanded in the region of the shift minimum. This plot reveals a clear difference between the low-temperature and high-temperature regions. On the high-density, low-temperature side of the minimum, isobars and isotherms are not coincident and

TABLE I. ^{133}Cs Knight-shift isobars.

$T(^{\circ}\text{C})$	Knight shift (%)				
	$P = 30$ bars	90	120	500	900
55	1.472	1.474	1.476	1.492	1.512
150	1.449		1.450	1.464	1.479
200	1.436		1.436	1.452	1.464
254	1.424		1.427	1.440	1.455
300	1.415		1.418	1.429	1.440
400	1.405		1.405	1.414	
500	1.400		1.400	1.403	
600	1.397		1.395	1.396	
700	1.398		1.399	1.393	
800	1.407	1.411	1.406	1.392	
895	1.420		1.414		
990	1.434	1.430	1.424		
1083	1.454	1.440	1.439		
1176	1.479	1.459	1.459		
1269		1.486	1.482		
1363		1.504	1.518		
1456		1.564	1.679		
1503		1.581			
1549		1.660			
1571		1.701			
1590		1.768			

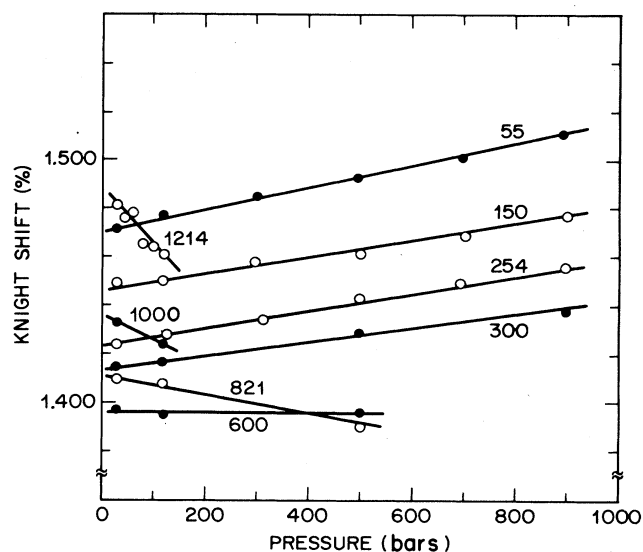


FIG. 5. ^{133}Cs Knight shifts vs pressure from isothermal measurements at the indicated temperatures ($^{\circ}\text{C}$).

there is an explicit negative temperature dependence for the shift at constant volume. The constant-volume temperature coefficient, $(\partial \ln K / \partial T)_v$, is negative and about 65% greater than the corresponding value for solid cesium (Table II). In contrast, at low densities the isobars and isotherms are coincident within experimental error. This has the important implication that the increase in the Knight shift on approaching the critical region is primarily due to the reduction of the density with the explicit temperature dependence playing a minor role.

B. Relaxation rates

^{133}Cs nuclear relaxation rates are presented in Fig. 8 plotted against temperature for various pressures. As discussed in the previous section, these rates are the observed inverse free-induction decay lifetimes corrected for

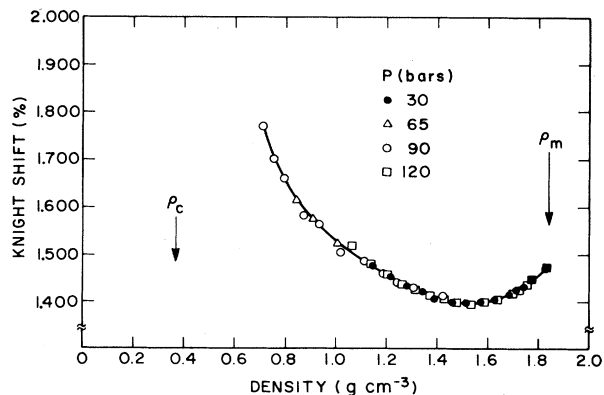


FIG. 6. Isobaric ^{133}Cs Knight shifts vs density at various pressures. Arrows indicate densities at melting and critical points.

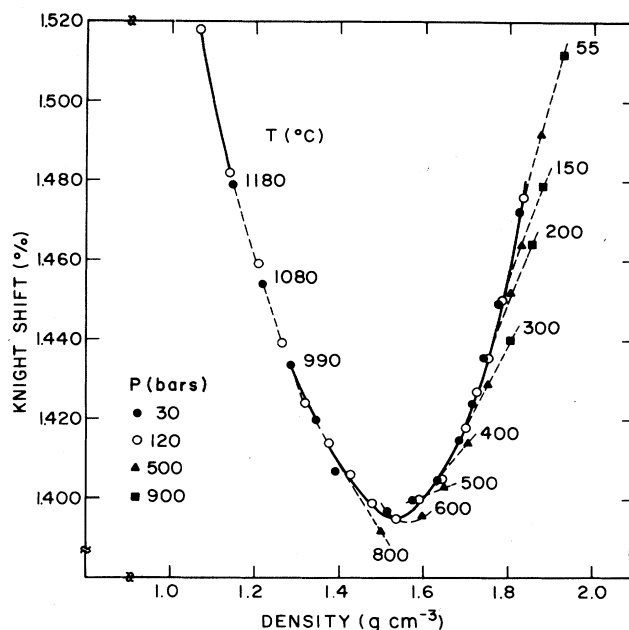


FIG. 7. ^{133}Cs Knight shifts vs density. Dashed lines are isotherms at the indicated temperatures. Solid line is isobar at 120 bars.

inhomogeneous broadening. We confirmed by direct measurement of the spin-lattice relaxation times, $1/T_1$, that the corrected value T_2 equals T_1 in the low-temperature range. As shown in Fig. 8, the quantity $1/T_2 T$ is roughly constant up to 800 $^{\circ}\text{C}$ then rises sharply with further heating toward the critical region. Because of poor signal-to-noise ratios at the highest temperatures, we were able to obtain reproducible data for the relaxation rate only to 1500 $^{\circ}\text{C}$, roughly 100 $^{\circ}\text{C}$ lower than the highest Knight-shift measurement. We were unable to

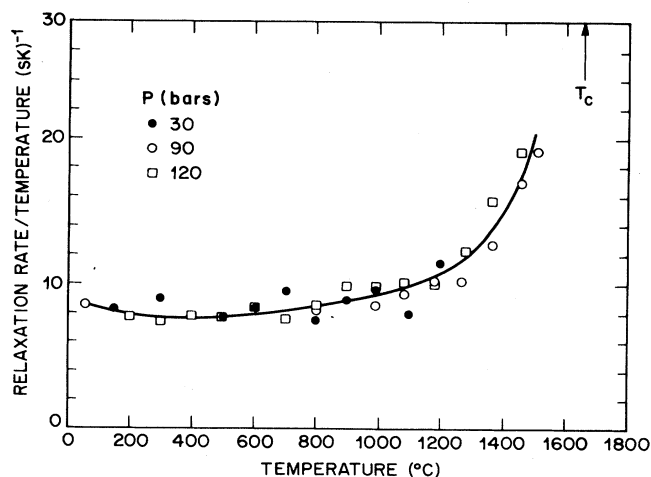


FIG. 8. ^{133}Cs nuclear relaxation rates/temperature, $1/T_2 T$, vs temperature at various pressures.

resolve the isothermal pressure dependence of the relaxation rate at any temperature.

IV. ANALYSIS AND INTERPRETATION

A. Theory

In this section we briefly summarize the basic theoretical expressions for NMR shifts and relaxation in fluid metals in an appropriate formulation for interpretation of our results.⁴¹ We place particular emphasis on the effects of electron-electron interactions on the magnetic response of the electrons.

The dominant coupling between the nuclear-spin system and the conduction electrons is the magnetic contact hyperfine interaction

$$H_c = \frac{8\pi}{3} \gamma_n \gamma_e \hbar^2 \sum_j \mathbf{I}^j \cdot \mathbf{S}(\mathbf{R}_j), \quad (3)$$

where \mathbf{I} and \mathbf{S} are the nuclear and electronic spins, respectively, and γ_n and γ_e are the corresponding gyromagnetic ratios. The summation is taken over all nuclear sites \mathbf{R}_j in the liquid. The consequences of the hyperfine interaction for NMR, namely shifts of the resonance frequency and nuclear-spin relaxation, are governed by different contributions to the generalized magnetic susceptibility

$$\chi(q, \omega) = \chi'(q, \omega) + i\chi''(q, \omega). \quad (4)$$

The Knight shift is proportional to the uniform, static limit of the real part of the generalized susceptibility $\chi'(0, 0)$:

$$K \equiv \frac{\Delta H}{H_0} = \frac{8\pi}{3} \langle |\psi(0)|^2 \rangle_F \Omega \chi'(0, 0), \quad (5)$$

where $\langle |\psi(0)|^2 \rangle$ is the electronic charge density at the nucleus, averaged over all states at the Fermi energy. The wavefunctions are normalized in the atomic volume Ω and $\chi'(0, 0)$ is the susceptibility per unit volume.

Fluctuations of the local hyperfine field at the nuclear resonance frequency ω_0 are responsible for longitudinal or spin-lattice relaxation. The relaxation rate depends on an integral over the transverse components of the imaginary part of the generalized susceptibility

$$\frac{1}{T_1} = \frac{32}{9} \langle |\psi(0)|^2 \rangle_F^2 \gamma_n^2 \gamma_e^2 kT \Omega^2 \omega_0^{-1} \int dq q^2 \chi''(q, \omega_0)_{\pm}. \quad (6)$$

In metals, the fluctuations are fast compared with the inverse nuclear Larmor frequency $1/\omega_0$ so that "extreme narrowing" conditions apply and $1/T_1 = 1/T_2$.

1. Noninteracting electrons

For noninteracting electrons, the uniform, static susceptibility is just the Pauli susceptibility

$$\chi'_0(0, 0) = \frac{1}{2} (\gamma_e \hbar)^2 N(E_F), \quad (7)$$

where $N(E_F)$ is the density of states at the Fermi level for a single direction of spin. The integral in Eq. (6) over the dynamic susceptibility can be evaluated explicitly for

noninteracting electrons in the low-frequency limit to yield

$$\omega_0^{-1} \int dq q^2 \chi''_0(q, \omega_0)_{\pm} = 2\pi^3 \gamma_e^2 \hbar^3 [N(E_F)]^2. \quad (8)$$

Substitution of Eq. (8) in Eq. (6) yields the familiar Korringa expression⁴² for the relaxation rate

$$\frac{1}{T_1} = \frac{64}{9} \pi^3 \hbar^3 \gamma_n^2 \gamma_e^2 \langle |\psi(0)|^2 \rangle_F^2 \Omega^2 kT [N(E_F)]^2, \quad (9)$$

and the combination of Eqs. (5), (7), and (9) leads to the Korringa relation between the relaxation rate and the Knight shift

$$\left[\frac{1}{T_1} \right]_{\text{Korringa}} = \left[\frac{4\pi k}{\hbar} \right] \left[\frac{\gamma_n}{\gamma_e} \right]^2 K^2 T. \quad (10)$$

It can be seen from Eqs. (5) and (6) that the Korringa relation, Eq. (10), expresses a particular relationship between the integral of the q -dependent dynamic susceptibility and the static, uniform susceptibility for noninteracting electrons

$$\omega_0^{-1} \int dq q^2 \chi''_0(q, \omega_0)_{\pm} = \left[\frac{8\pi^3}{\gamma_e^2 \hbar} \right] [\chi'_0(0, 0)]^2. \quad (11)$$

We now consider how this relationship is changed by interactions.

2. Interacting electrons

The magnetic effects of electron-electron interactions are manifest as enhancements of the generalized susceptibility. These fall into two classes: a cooperative exchange-correlation enhancement of the local magnetic field, and correlation enhancement of the effective mass or density of states at the Fermi level. The first is exemplified by the Stoner model and the second by the Brinkman-Rice model of a highly correlated metal.

(a) *Stoner enhancement.* The effects of interactions in alkali metals under ordinary conditions are usually described in terms of the Stoner model of exchange-correlation enhancement.⁶ The generalized susceptibility is expressed in a molecular field or random-phase approximation (RPA)

$$\chi(q, \omega) = \frac{\chi_0(q, \omega)}{1 - V_{xc}(q)\chi_0(q, \omega)}, \quad (12)$$

in which $V_{xc}(q)$ is proportional to the q -dependent exchange-correlation potential. The enhanced static, uniform susceptibility then takes the simple form

$$\chi'(0, 0) = \frac{\chi'_0(0, 0)}{1 - \alpha}, \quad (13)$$

where $\alpha = V_{xc}(0)\chi'_0(0, 0)$. Enhancement of the imaginary part of the dynamic susceptibility is q dependent and at low frequencies may be written

$$\chi''(q, \omega) = \frac{\chi''_0(q, \omega)}{[1 - \alpha f(q)]^2}, \quad (14)$$

where the q -dependence $f(q)$ is determined by the form

of the exchange-correlation potential and the nonuniform susceptibility for noninteracting electrons

$$f(q) = \frac{V_{xc}(q)\chi'_0(q,0)}{V_{xc}(0)\chi'_0(0,0)} \quad (15)$$

The q -dependent enhancement of $\chi''(q, \omega_0)$ leads to breakdown of the Korringa relation, Eq. (10) or Eq. (11). As shown first by Moriya,⁴³ substitution of specific functions for $V_{xc}(q)$ and $\chi'_0(0,0)$ gives a quantitative relation between the Korringa ratio

$$\eta \equiv \left[\frac{1}{T_1} \right] / \left[\frac{1}{T_1} \right]_{\text{Korringa}} = \frac{\omega_0^{-1} \int dq q^2 \chi''(q, \omega_0)_{\pm}}{(8\pi^3 / \gamma_e^2 \hbar) [\chi'(0,0)]^2}, \quad (16)$$

and the static enhancement parameter α .⁴⁴ For cesium at normal densities, the experimental Korringa ratio interpreted with Shaw's exchange-correlation potential⁴⁵ yields a value $\alpha=0.44$, or, using Eq. (13), a uniform enhancement of about 1.8. This is a typical value for alkali metals.

The function $f(q)$ is a decreasing function of q in simple metals and the enhancement in this model is therefore lower at finite q than at $q=0$. Thus, the Stoner enhancement is ferromagnetic in the sense that the largest enhancement occurs for the uniform magnetization. While the quantitative relation between η and α depends on the form of the exchange-correlation potential, inspection of Eqs. (13), (14), and (15) shows that the Korringa ratio, Eq. (16), is less than 1 and η decreases further the more the static enhancement α increases.

(b) *Correlation enhancement.* The enhancement of the susceptibility by correlation was described by Brinkman and Rice⁷ using a variational method created by Gutzwiller.⁸ Unlike the Stoner model, the Brinkman-Rice description explicitly introduces the role of the atoms. The majority of sites in the highly correlated metal are assumed to be instantaneously singly occupied leaving only a small fraction f doubly occupied. Brinkman and Rice showed that the effective mass in the highly correlated metal is enhanced according to

$$m^*/m_e = 1/2f. \quad (17)$$

The enhancement leads to a new degeneracy temperature T_d reduced relative to the Fermi temperature T_F of the noninteracting system

$$T_d = 2fT_F. \quad (18)$$

Enhancement in the highly correlated metal differs in two important respects from Stoner enhancement. First, both the susceptibility and electronic specific heat are enhanced, whereas Stoner enhancement affects only the susceptibility. While enhancement of the specific heat is unlikely to be observed in expanded liquid metals due to the dominance of the "lattice" specific heat, this enhancement is commonly seen in heavy fermion metals.⁴⁶ The second important difference is that the static, uniform susceptibility of the highly correlated metal saturates at the Curie value as the experimental temperature ap-

proaches the degeneracy temperature T_d . In contrast, the Stoner susceptibility, Eq. (13), can increase without limit as $\alpha \rightarrow 1$ and, in fact, this divergence indicates the onset of ferromagnetism. The limitation of the susceptibility to the Curie value is important for expanded cesium because of the high experimental temperatures and possible reduction of the degeneracy temperature by correlation enhancement.

Calculations for the Hubbard model indicate that the ground state of the highly correlated metal is antiferromagnetic.⁹ Likewise, band calculations for crystalline atomic hydrogen show a progression from paramagnetic metal to antiferromagnetic metal to antiferromagnetic insulator as the crystal is expanded. The nonuniform susceptibility of an antiferromagnetic metal should have a maximum at a finite q value corresponding to the ordering wavelength. Direct calculations of $\chi'(q,0)$ by Kelly and Glötzel¹³ show, indeed, that the susceptibility of hydrogen at the zone boundary exceeds that at $q=0$. The calculations for expanded alkali metals, however, are contradictory. Band calculations for expanded lithium by Min *et al.*¹¹ indicate that a ferromagnetic ground state is slightly favored and they argue that a similar situation should hold for the other alkali metals. Kelly and Glötzel,¹³ in contrast, found that antiferromagnetic order sets in at a higher density than ferromagnetic order as various crystalline structures of cesium are expanded.

Development of a tendency toward antiferromagnetic ordering has an important consequence for nuclear relaxation. According to Eq. (16) and the arguments given in the preceding section, enhancement of $\chi''(q, \omega)$ at finite q in excess of the enhancement at $q=0$ should lead to an increase of the Korringa ratio relative to the value $\eta=1$ expected in the noninteracting limit. Since, as we have seen, the Korringa ratio is reduced for Stoner (ferromagnetic) enhancement, measurement of η provides a means of distinguishing between the two types of enhancement.

B. Characteristics of the high-density liquid

The electronic structure and magnetic properties of liquid cesium near the melting point are very similar to those of the solid just below the melting point. The Knight shift, for example, decreases by only 1.8% on melting, and the spin-lattice relaxation rate changes by less than 10%. The Korringa enhancements are 0.58 and 0.61 in the solid⁴⁷ and liquid, respectively, showing that the susceptibility enhancement is only slightly affected by melting. With the exception of the isochoric temperature coefficient, $(\partial \ln K / \partial T)_v$, the various temperature and pressure coefficients of the Knight shift in the liquid lie within 20% of their values for solid cesium (Table II).

These small changes in magnetic properties at T_m correlate with strong indications that relatively little change in the local atomic arrangement occurs during melting. The molar volume increases by only 2.5%, for example, and the average near-neighbor distance in the liquid, 5.31 Å,⁴⁸ is identical to the near-neighbor distance in bcc cesium about 40 °C below T_m .⁴⁹ The density of states at the Fermi level in solid cesium is strongly influenced by the d states which lie mostly above E_F .

Band calculations⁵⁰ give a value $m^* = 1.76$ for the effective mass. The small changes in magnetic properties on melting show that this "band-structure" enhancement of the density of states persists in the liquid. Most of the change in Knight shift on melting can be attributed to the small volume change at the phase transition viewed as an extension of the thermal expansion of the solid. Accordingly, we calculate the change at the melting point ΔK using the volume coefficient of the Knight shift measured for the solid,

$$\frac{\Delta K}{K_{\text{solid}}} = \left[\frac{\Delta V}{V_{\text{solid}}} \right] \left[\frac{\partial \ln K}{\partial \ln V} \right]_{\text{solid}} = -1.6\% , \quad (19)$$

which can be compared with the observed value -1.8% . This is strong evidence that the electric and magnetic properties are determined mainly by the volume and local distribution of near neighbors and are not strongly influenced by the loss of long-range order on melting. This basic idea motivates the use of crystalline models to calculate the electronic structure and properties of expanded liquid cesium.^{13,51}

The volume dependence of the shift in the solid and dense liquid results mainly from the decrease in density of states as the Fermi level moves away from the d states. Close to T_m the isothermal volume dependence is very similar in liquid and solid. This is in agreement with the basic assumption of the "uniform fluid model" (UFM) according to which the structure is unaffected by pressure except for a simple scaling of distances by $V^{1/3}$.⁵² Recent neutron studies of liquid cesium⁵³ show that the UFM is valid close to T_m , but that it breaks down dramatically at higher temperatures. This is completely consistent with the data shown in Fig. 5 which display a striking change in the isothermal volume dependence of the shift between 300 and 600°C.

Even near the melting point, however, the explicit tem-

TABLE II. ¹³³Cs differential Knight-shift coefficients in solid and liquid cesium near the melting point.

	Solid	Liquid
$\left. \frac{\partial \ln K}{\partial T} \right\}_P$	$-1.85 \times 10^{-4} K^{-1a,b}$	$-1.66 \pm 0.10 \times 10^{-4} K^{-1}$
$\left. \frac{\partial \ln K}{\partial P} \right\}_T$	$3.4 \times 10^{-5} \text{bar}^{-1c}$	$3.2 \pm 0.2 \times 10^{-5} \text{bar}^{-1}$
$\left. \frac{\partial \ln K}{\partial \ln V} \right\}_T$	$-0.62^{c,d}$	-0.48 ± 0.07
$\left. \frac{\partial \ln K}{\partial T} \right\}_V$	$-0.7 \times 10^{-4} K^{-1e}$	$-1.16 \pm 0.09 \times 10^{-4} K^{-1}$

^aB. R. McGarvey and H. S. Gutowsky, *J. Chem. Phys.* **21**, 2114 (1953).

^bH. T. Weaver and A. Narath, *Phys. Rev. B* **1**, 973 (1970).

^cG. B. Benedek and T. Kushida, *J. Phys. Chem. Solids* **5**, 241 (1958).

^dM. S. Anderson, E. J. Gutman, J. R. Packard, and C. A. Swenson, *J. Phys. Chem. Solids* **30**, 1587 (1969).

^eReference (c) corrected in T. Muto, S. Kobayasi, M. Watanabe, and H. Kozima, *J. Phys. Chem. Solids* **23**, 1303 (1962).

perature dependence of the Knight shift in liquid cesium is substantially larger than in the solid. Furthermore, the explicit temperature dependence decreases rapidly with temperature in the liquid, whereas in the solid it is nearly the same at helium temperatures⁵⁴ and close to the melting point.⁵⁵ The origin of the explicit temperature dependence is not well understood in either liquid or solid, although it may be partially explained by effective thermal averaging of the structure factor and a resulting tendency toward a more free-electron-like density of states at high temperature. A theory based on this effect was quite successful in explaining the unusually strong temperature dependence of the Knight shift in solid cadmium.⁵⁶

The divergence with increasing temperature of liquid-state properties from those of the solid may reflect in part an essential difference in the nature of thermal expansion and thermal excitations in the two phases. Whereas thermal expansion of the crystal is due to anharmonic lattice vibrations that lead to increased average interatomic separations, neutron studies of liquid cesium⁵⁷ and rubidium⁵⁸ show that expansion of the liquid is mainly due to reduced numbers of near neighbors. Only slight increases in the interatomic distances are observed. In other words, as the liquid expands with increasing temperature, it undergoes a continuous change of structure. Continuous structural evolution is, of course, forbidden by the requirements of crystalline symmetry in the solid, and it is therefore not surprising to find that significant differences develop in the temperature and pressure dependence of electronic structure and properties of solid and liquid, even with relatively modest increases in temperature.

C. The static, uniform susceptibility in expanded cesium

The behavior of the static, uniform susceptibility reveals that significant changes in the electronic properties of cesium develop at low density. In Fig. 9 we show the volume electronic susceptibility extracted from Freyland's measurements²³ of the mass susceptibility along the coexistence curve. To obtain the electronic

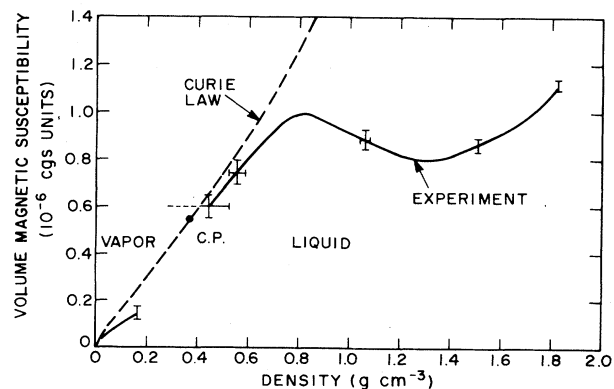


FIG. 9. Spin susceptibility (per unit volume) vs density along liquid-gas coexistence curve (Ref. 23). Dashed line indicates Curie law along coexistence curve calculated for one electron per atom.

paramagnetic contribution from the total susceptibility, we corrected for diamagnetism using a value⁵⁹ $-35 \times 10^{-6} \text{ cm}^3/\text{mole}$ for the ionic diamagnetism and values of the electronic diamagnetic susceptibility calculated from the theory of Kanazawa and Matsudawa.⁶⁰ The dominant features of the data shown in this figure are a gradual decrease of $\chi'(0,0)$ as the density decreases from the normal value at the melting point, a sharp rise as the density falls below about 1.5 g/cm^3 , and a decrease in the lowest-density range.

Since the Stoner model adequately explains the enhancement of $\chi'(0,0)$ in the solid and normal liquid, it is natural to ask whether increased enhancement at low density can be explained within the framework of this theory. There is persuasive evidence that this is not the case. First, theoretical calculations^{13,51} for various low-density cesium crystal structures offer no indication that the density of states (per unit volume) at the Fermi level increases as the density decreases. To take account of the structural evolution of the expanding liquid, band calculations^{13,15} were carried out for various structures having different near-neighbor coordination numbers with a constant value of the near-neighbor distance. This feature of the structural evolution was also exploited by Franz⁶¹ for a model of expanded metals viewed as an "alloy" of atoms and vacancies. These models predict either decreasing^{13,51} or constant⁶¹ densities of states at the Fermi level and accordingly, Eqs. (7) and (13) do not predict increased enhancement of the volume susceptibility at low density unless the Stoner parameter α increases sharply. The latter possibility is precluded, however, by the behavior of the Korringa enhancement shown in Fig. 10. We observed that η increases significantly in the low-density range and reaches values slightly greater than 1 at the lowest densities. The same trend was observed for liquid sodium over a more limited density range by Bottyan *et al.*⁶² Since the Stoner picture outlined in Sec. IV A 2 predicts a decrease in η if α increases, an increase in the Korringa enhancement is inconsistent with increased enhancement of $\chi'(0,0)$ on the conventional model.

Finally, we consider the decrease of the susceptibility

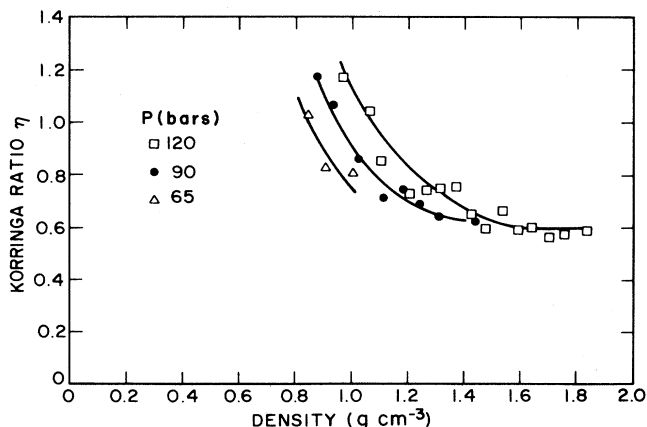


FIG. 10. Korringa ratio η vs density at the indicated pressures.

when the density falls below 0.8 g/cm^3 . As may be seen in Fig. 9, $\chi'(0,0)$ is limited by Curie value for densities below this value. This behavior is not expected for Stoner enhancement and indicates that the low-density enhancement is due to a reduced degeneracy temperature as in the Brinkman-Rice model.²⁵ Chapman and March⁶³ have recently shown how this crossover from Stoner to Brinkman-Rice enhancement follows from the finite temperature extension⁶⁴ of the theory of Brinkman and Rice. They conclude that cesium is highly correlated for densities below $\sim 0.8 \text{ g/cm}^3$.

The preceding analysis has been developed using concepts familiar from the study of condensed metals at low temperatures. The influence of their high- experimental temperatures has been introduced only through the Curie law limitation of the susceptibility. We believe this approach is justified by the essentially metallic character of cesium throughout the range covered in this investigation. For example, the minimum value of the electrical conductivity in our experimental range is about $700 (\Omega \text{ cm})^{-1}$, and the Hall coefficient remains close to the free-electron value for one electron per atom down to at least $\rho = 1.1 \text{ g/cm}^3$,⁶⁵ the lowest density measured. A complementary theoretical approach developed by Alekseev and Iakubov⁶⁶ begins with a description of the low-density, high-temperature gas as a weakly ionized plasma. Hernandez⁶⁷ has adopted this point of view and calculated the thermodynamic equilibria for formation of various polyatomic species as the density of the gas is increased. This approach provides a consistent interpretation of the electrical and magnetic properties at densities up to the critical region and predicts, in particular, an important role for the diamagnetic dimers in this range. However, the high-density limit of this theory is a uniform metal ("jellium"), and thus the model does not include the important ion-ion and electron-ion correlations that characterize the developing condensed state. Chapman and March⁶³ have pointed out that the magnetic susceptibility in this region shows a marked difference from that of jellium and they attribute this to the substantial influence of electron-ion interactions on the electronic structure.

D. The dynamic, nonuniform susceptibility in expanded cesium

We have discussed the breakdown of the Stoner enhancement description of expanded cesium in the previous section. We now consider more explicitly the implications for $\chi''(q, \omega_0)_\pm$ of the observed increase in the Korringa ratio at low densities. Using the low-frequency expression for the dynamic, nonuniform susceptibility in the noninteracting system⁶⁸

$$\chi''(q, \omega_0)_\pm = \frac{8\pi^3}{\gamma_e^2 \hbar^2} [\chi'_0(0,0)]^2 \frac{\hbar \omega_0}{2q_F^2} \frac{1}{q}, \quad (20)$$

one can show from Eq. (16) that the Korringa ratio may be written

$$\eta = \frac{1}{2q_F^2} \int_0^{2q_F} dq qg(q). \quad (21)$$

The function $g(q)$ provides a general description of the q dependence of $\chi''(q, \omega_0)_\pm$ relative to that of the noninteracting system:

$$\frac{\chi''(q, \omega_0)_\pm}{\chi''_0(q, \omega_0)_\pm} = \frac{\chi''(0, \omega_0)_\pm}{\chi''_0(0, \omega_0)_\pm} g(q). \quad (22)$$

In the conventional Stoner description, Eq. (14) gives

$$g_s(q) = (1 - \alpha)^2 / [1 - \alpha f(q)]^2. \quad (23)$$

It is the monotonic decrease in $g_s(q)$ that leads to values $\eta < 1$ in cases of Stoner enhancement.

The data presented in Fig. 10 show that η increases strongly as the density falls below about 1.4 g/cm³ and reaches values in excess of 1 at the lowest densities. It is evident from Eq. (21) that values of $\eta > 1$ require that $g(q)$ increase and exceed $g(0)$ in some range of nonzero q . Such behavior corresponds to a change in the enhancement of the dynamic, nonuniform susceptibility from ferromagnetic in the normal metal to antiferromagnetic enhancement in the expanded metal.

To get a semiquantitative description of the antiferromagnetic enhancement, we have modeled the evolution of $g(q)$ using a function characterized by increased enhancement in the vicinity of $q = 2q_F$

$$g(q) = g_s(q) \left[1 + \left(\frac{q}{q + q_F} \right) \frac{\lambda}{1 + (q - 2q_F)^2 \lambda^2} \right]. \quad (24)$$

This function is plotted in Fig. 11 for 3 sets of parameters that yield η values in the range 0.6–1.2 measured in our experiments. Since η depends only on the integral of $g(q)$ as shown by Eq. (21), it is obvious that the particular form chosen for Eq. (24) has no special significance. We could have chosen any function in which the high- q enhancement occurs at a nonzero value of q in the range $0 < q < 2q_F$. The presence of a peak in $g(q)$ and η values greater than 1 implies a tendency for anticorrelation of spins or, in other words, formation of slightly underdamped spin-density waves in the low-density metal. For a spin-density wave of wavelength $2/q_F$, corresponding to Eq. (24) and Fig. 11, a correlation length comparable with the wavelength and interatomic spacing yields the η values observed at the lowest densities.

E. Conduction electron wave functions

The average density of Fermi energy electrons at the nucleus, $\langle |\Psi(0)|^2 \rangle_F$, can be obtained from the Knight shift and susceptibility results using Eq. (5). Susceptibility data²³ are available only along the liquid-gas coexistence curve so we have extrapolated our Knight-shift data to the coexistence curve using the density dependence shown in Figs. 6 and 7. The paramagnetic, electronic susceptibility extracted from the data of Freyland is that shown in Fig. 9. For convenience we follow the convention of expressing the charge density at the nucleus in units of the atomic value $\xi = \langle |\Psi(0)|^2 \rangle_F / |\Psi(0)|_a^2$, where $|\Psi(0)|_a^2 = 2.58 \times 10^{25} \text{ cm}^{-3}$.⁶⁹ The result plotted in Fig. 12 shows a density-independent value $\xi \sim 0.5$ at high densities, but ξ decreases markedly when

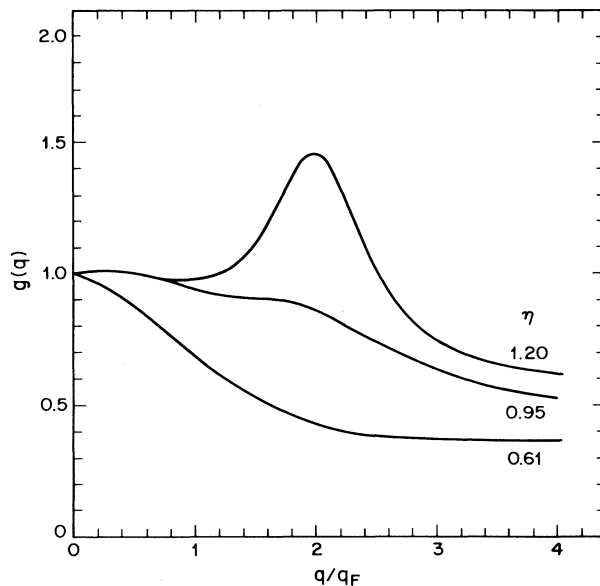


FIG. 11. Model form of $g(q)$, Eq. (24), giving indicated values of the Korrington ratio. Parameters $(\alpha, \lambda q_F)$ are (0.40, 0.001), (0.33, 1.0), and (0.25, 2.0) for η -values 0.61, 0.95, 1.20, respectively.

ρ drops below about 1.4 g/cm³. At the lowest densities, ξ reaches a minimum value of about 0.28 and then starts to increase.

The density dependence of ξ shown in Fig. 12 is contrary to naive expectations. It is obvious from its definition that ξ must approach the value 1 in the dilute (atomic) limit. However, the unexpected decrease of ξ in the range 1.4–0.8 g/cm³ shows that this does not occur monotonically. The band calculations fail to account for this effect since they indicate a simple monotonic increase of ξ from the value in the high-density metal to the atomic value.^{13,51} The reduction in ξ cannot be due to spin pairing in dimers or other species since ξ is defined to be the charge density of only those electrons contributing to

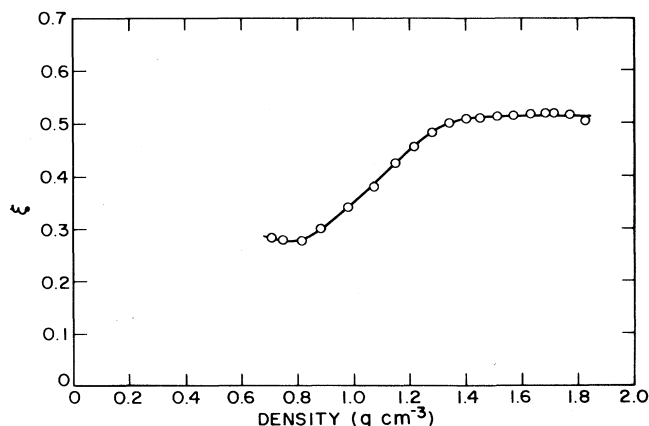


FIG. 12. Normalized charge density parameter ξ vs from susceptibility (Ref. 23) and ¹³³Cs Knight shifts extrapolated to liquid-gas coexistence curve.

the susceptibility. Rather, the data show that there is a substantial movement of conduction electron charge away from the ions in the intermediate density range. The minimum in ξ at about 0.8 g/cm^3 indicates that this trend is reversed at very low density.

V. SUMMARY: EVOLUTION OF THE ELECTRONIC STRUCTURE AND PROPERTIES OF EXPANDED LIQUID CESIUM

Liquid cesium near the melting point may be considered a normal liquid metal with properties typical of the condensed state. The small changes of most electronic properties on melting show that the electronic structure of the liquid is quite similar to that of bcc crystalline cesium close to the melting point. This remains basically true during expansion to densities in the range $1.4\text{--}1.6 \text{ g/cm}^3$ except for gradual changes in temperature and pressure coefficients from their solid-state values. These changes provide an indication of the fundamentally different character of thermal expansion in the solid and liquid states. Throughout this range of initial expansion, the Korringa enhancement parameter remains constant and the susceptibility enhancement is consistent with the conventional Stoner theory. The distribution of electronic charge is affected little in this range and maintains a roughly constant value $\xi=0.5$ for $\rho > 1.4 \text{ g/cm}^3$.

As the density is reduced below about $1.4\text{--}1.6 \text{ g/cm}^3$, qualitative changes develop and the liquid takes on unusual electronic characteristics. The susceptibility enhancement increases sharply, the Korringa relation breaks down, indicating a shift from ferromagnetic to antiferromagnetic enhancement, and the wave functions spread out so as to cause a substantial reduction of charge density at the nucleus. The latter effect is reversed only at the lowest densities, below 0.8 g/cm^3 , roughly twice the critical density. Despite these changes, cesium retains metallic conductivity values to below 0.7 g/cm^3 and the Hall coefficient is within 10% of the free-electron value down to at least 1.1 g/cm^3 . The electronic spin susceptibility at the lowest densities follows the Curie law expected for 1 electron/atom obeying classical Boltzmann statistics. Although the experimental value for the spin susceptibility is subject to some uncertainty because of the necessary diamagnetic correction, there is little evidence of a substantial fraction of paired spins in this range of the subcritical liquid.

The magnetic properties at low density are not explicable by extension of the conventional Stoner enhance-

ment mechanism. Rather, cesium becomes a highly correlated metal with antiferromagnetic spin fluctuations. As such it is related to other highly correlated systems including high-temperature superconducting cuprates. Indeed, the resonance properties of the latter are qualitatively similar in that they are marked by strong enhancement of the dynamic susceptibility relative to the uniform, static susceptibility.⁷⁰ We suggest, nevertheless, that the electronic structure of expanded cesium is governed not only by the mean carrier density and approach to the metal-nonmetal transition, but that it is related also to the structural evolution peculiar to expansion of a liquid approaching the critical point. An expanded liquid metal is fundamentally different in this respect from a dilute metal formed by solid solution such as Si:P. In the latter case, the electron centers are fixed and there is essentially no interplay between the spatial arrangement of these centers and the changes in electronic structure which occur as their density is varied.

In the case of alkali metals, the symmetry of the wave functions may play an important role in the interplay between liquid structure and electronic properties. This is because the local environment becomes increasingly anisotropic as the liquid expands and the local coordination number decreases. For a high concentration of "vacancies," the spherically symmetric 6s wave functions can no longer fit neatly into nonoverlapping Wigner-Seitz-like cells as they can in the highly coordinated normal liquid metal. Thus, a competition develops between the kinetic energy to be gained by expansion of the wave function into the vacant spaces in the liquid structure and the increases of Coulomb energy in the region of overlap between near neighbors. Overlap of neighboring 6s functions necessarily favors anticorrelation of the spins on adjacent atoms. From this point of view, it is not surprising that spreading of the wave functions, indicated by decreasing values of ξ , coincides with development of antiferromagnetic exchange enhancement of the nonuniform susceptibility. As the liquid breaks up into smaller and smaller clusters of atoms near the critical point, this process merges naturally into formation of a substantial fraction of spin-paired dimers in the vapor phase. Such species are the fluid-state counterparts of effects such as the Peierls dimerization that frequently accompanies the onset of antiferromagnetic order in crystals at low temperatures or, indeed, the formation of molecular hydrogen. Thus, although the microscopic electron characteristics in the critical region remain to be explored more completely, we can begin to discern the outlines of the continuous evolution to the nonmetallic state of the vapor.

¹N. F. Mott, Proc. Phys. Soc. London **62**, 419 (1949).

²J. Hubbard, Proc. R. Soc. London, Ser. A **277**, 237 (1964); **281**, 401 (1964).

³P. W. Anderson, Phys. Rev. **115**, 2 (1959).

⁴For a recent discussion of compressed hydrogen, see D. M. Ceperley and B. J. Alder, Phys. Rev. B **36**, 2092 (1987).

⁵See, for example, J. F. Hirsch, E. Loh, D. J. Scalapino, and S. Tang, Physica **153**–**155**, 549 (1988).

⁶See, for example, V. L. Moruzzi, J. F. Janak, and A. R. Williams, *Calculated Electronic Properties of Metals* (Pergamon, New York, 1978).

⁷W. F. Brinkman and T. M. Rice, Phys. Rev. B **2**, 4302 (1970).

- ⁸M. C. Gutzwiller, *Phys. Rev.* **137**, A1726 (1965).
- ⁹See, for example, N. F. Mott, *Metal-Insulator Transitions* (Taylor and Francis, London, 1974), Chap. 4.
- ¹⁰L. M. Sander, H. B. Shore, and J. H. Rose, *Phys. Rev. B* **24**, 4879 (1981).
- ¹¹B. I. Min, T. Oguchi, H. J. F. Jansen, and A. J. Freeman, *Phys. Rev. B* **33**, 324 (1986).
- ¹²P. J. Kelly, O. K. Anderson, and T. M. Rice (unpublished).
- ¹³P. J. Kelly and D. Glözel, *Phys. Rev. B* **33**, 5284 (1986).
- ¹⁴J. P. Stone, C. T. Ewing, J. R. Spann, E. W. Steinkueller, D. D. Williams, and R. R. Miller, *J. Chem. Eng. Data* **11**, 309 (1966).
- ¹⁵G. Franz, Ph.D. dissertation, University of Marburg, 1980.
- ¹⁶S. Jüngst, B. Knuth, and F. Hensel, *Phys. Rev. Lett.* **55**, 2160 (1985).
- ¹⁷H. Renkert, F. Hensel, and E. U. Franck, *Ber. Bunsenges. Phys. Chem.* **75**, 507 (1971).
- ¹⁸H. P. Pfeifer, W. Freyland, and F. Hensel, *Ber. Bunsenges. Phys. Chem.* **80**, 716 (1976); **83**, 204 (1979).
- ¹⁹G. Franz, W. Freyland, and F. Hensel, *J. Phys. (Paris) Colloq.* **41**, C8-70 (1980).
- ²⁰F. Noll, W.-C. Pilgrim, and R. Winter, *Z. Phys. Chem. Neue Folge* **156**, 303 (1988).
- ²¹L. Landau and J. Zeldovich, *Acta Physiochim. URSS* **18**, 194 (1943).
- ²²R. E. Goldstein and N. W. Ashcroft, *Phys. Rev. Lett.* **55**, 2164 (1985).
- ²³W. Freyland, *Phys. Rev. B* **20**, 5104 (1979).
- ²⁴W. Freyland, *J. Phys. (Paris) Colloq.* **41**, C8-74 (1980).
- ²⁵W. W. Warren, Jr., *Phys. Rev. B* **29**, 7012 (1984).
- ²⁶U. El-Hanany, G. F. Brennert, and W. W. Warren, Jr., *Phys. Rev. Lett.* **50**, 540 (1983).
- ²⁷W. W. Warren, Jr., U. El-Hanany, and W. W. Warren, Jr., *J. Non-Cryst. Solids* **61-62**, 23 (1984).
- ²⁸W. W. Warren, Jr., in *Amorphous and Liquid Metals*, Vol. 118 of *Nato Advanced Study Institute, Series E*, edited by E. Lüscher, G. Fritsch, and G. Jaccucci (Martinus Nijhoff, Dordrecht, 1987), p. 304.
- ²⁹F. Hensel, S. Jüngst, B. Knuth, H. Uchtmann, and M. Yao, *Physica* **139-140B**, 90 (1986).
- ³⁰High purity grade (99.9+%), Callery Chemical Co., Callery, PA 16024.
- ³¹Tyco Saphikon, Milford, NH 03055.
- ³²I. P. Host, E. F. W. Seymour, and G. A. Styles, *J. Nucl. Mater.* **35**, 55 (1970).
- ³³E. I. DuPont Co., Wilmington, DE 19898.
- ³⁴W. G. Clark, *Rev. Sci. Instrum.* **35**, 316 (1964).
- ³⁵A. Kornblit, Ph.D. thesis, Rutgers University, 1981 (unpublished).
- ³⁶Our shift calibration yielded a value $K = 1.477 \pm 0.001\%$ for liquid cesium at the melting point. When comparing this with the accepted value from the literature, $K = 1.46 \pm 0.01$ (Ref. 37), it is important to note that the original authors (Ref. 38) used a nonstandard definition of the Knight shift i.e., $K = (H_{\text{ref}} - H_{\text{met}}) / H_{\text{ref}}$, where H_{ref} and H_{met} are the resonant fields for the reference and metal samples, respectively. This choice of definition has apparently not been taken into account in subsequent quotations of the shift value. When the conventional definition $K = (H_{\text{ref}} - H_{\text{met}}) / H_{\text{met}}$ is applied to the data of Ref. 38, one obtains a shift $K = 1.485 \pm 0.010\%$ that agrees within experimental error with our independently measured value.
- ³⁷G. C. Carter, L. H. Bennett, and D. J. Kahan, *Metallic Shifts in NMR* (Pergamon, Oxford, 1977), p. 182.
- ³⁸H. S. Gutowsky and B. R. McGarvey, *J. Chem. Phys.* **20**, 1472 (1952); B. R. McGarvey and H. S. Gutowsky, *ibid.* **21**, 2114 (1953).
- ³⁹J. A. Kaeck, *Phys. Rev. B* **5**, 1659 (1972).
- ⁴⁰G. B. Benedek and T. Kushida, *J. Phys. Chem. Solids* **5**, 241 (1958).
- ⁴¹For a more complete discussion see, for example, J. Winter, *Magnetic Resonance in Metals* (Oxford, London, 1971).
- ⁴²J. Korrington, *Phys.* **16**, 601 (1950).
- ⁴³T. Moriya, *J. Phys. Soc. Jpn.* **18**, 516 (1963).
- ⁴⁴The Korrington ratio η is usually denoted $K(\alpha)$ in this model to display explicitly the dependence on α . We have chosen the notation η to emphasize the generality of the Korrington ratio and to permit discussion outside the context of the Stoner model and Moriya's theory (Ref. 43).
- ⁴⁵R. W. Shaw, Jr. and W. W. Warren, Jr., *Phys. Rev. B* **3**, 1562 (1971).
- ⁴⁶See, for example, K. Andres, J. E. Graebner, and H. R. Ott, *Phys. Rev. Lett.* **35**, 1779 (1975).
- ⁴⁷A. Narath and H. T. Weaver, *Phys. Rev.* **175**, 373 (1968).
- ⁴⁸N. S. Gingrich and L. Heaton, *J. Chem. Phys.* **34**, 873 (1961).
- ⁴⁹W. B. Pearson, *A Handbook of Lattice Spacings and Structures of Metals and Alloys* (Pergamon, Oxford, 1964).
- ⁵⁰F. S. Ham, *Phys. Rev.* **128**, 82 (1962).
- ⁵¹W. W. Warren, Jr. and L. F. Mattheiss, *Phys. Rev. B* **30**, 3103 (1984).
- ⁵²P. A. Egelstaff, I. D. Page, and C. R. T. Heard, *J. Phys. C* **4**, 1453 (1971); P. A. Egelstaff, J. B. Suck, W. Gläser, R. McPhearson, and A. J. Teitsma, *J. Phys. (Paris) Colloq.* **41**, C8-222 (1980).
- ⁵³R. Winter, F. Hensel, T. Bodensteiner, and W. Gläser, *J. Phys. Chem.* **92**, 7171 (1988).
- ⁵⁴H. T. Weaver and A. Narath, *Phys. Rev. B* **1**, 973 (1970).
- ⁵⁵Ref. 39, as corrected in T. Muto, S. Kobayashi, M. Watanabe, and H. Kozima, *J. Phys. Chem. Solids* **23**, 1303 (1962).
- ⁵⁶R. V. Kasowski, *Phys. Rev.* **187**, 891 (1969).
- ⁵⁷R. Winter, F. Hensel, T. Bodensteiner, and W. Gläser, *Ber. Bunsenges. Phys. Chem.* **91**, 1327 (1987).
- ⁵⁸G. Franz, W. Freyland, W. Gläser, F. Hensel, and E. Schneider, *J. Phys. (Paris) Colloq.* **41**, C8-194 (1980).
- ⁵⁹G. W. Brindley and F. E. Hoare, *Trans. Faraday Soc.* **33**, 268 (1937); *Proc. Phys. Soc. London* **49**, 619 (1937).
- ⁶⁰H. Kanazawa and N. Matsudawa, *Prog. Theor. Phys.* **23**, 433 (1960).
- ⁶¹J. R. Franz, *Phys. Rev. B* **29**, 1565 (1984).
- ⁶²L. Bottyan, R. Dupree, and W. Freyland, *J. Phys. F* **13**, L173 (1983).
- ⁶³R. G. Chapman and N. H. March, *Phys. Rev. B* **38**, 792 (1988).
- ⁶⁴T. M. Rice, K. Ueda, H. R. Ott, and H. Rudigier, *Phys. Rev. B* **31**, 594 (1985).
- ⁶⁵U. Even and W. Freyland, *J. Phys. F* **5**, L104 (1975).
- ⁶⁶V. A. Alekseev and I. T. Iakubov, *Phys. Rep.* **96**, 1 (1983).
- ⁶⁷J. P. Hernandez, *Phys. Rev. A* **34**, 1316 (1986); *Phys. Rev. Lett.* **57**, 3183 (1986).
- ⁶⁸See, for example, S. Doniach, *Proc. Phys. Soc. (London)* **91**, 86 (1983).
- ⁶⁹P. Kusch and H. Taub, *Phys. Rev.* **75**, 1477 (1949).
- ⁷⁰R. E. Walstedt, W. W. Warren, Jr., R. F. Bell, G. F. Brennert, G. P. Espinosa, R. J. Cava, L. F. Schneemeyer, and J. V. Waszczak, *Phys. Rev. B* **38**, 9303 (1988).